

The discovery of two mildly-recycled binary pulsars in the Northern High Time Resolution Universe pulsar survey

M. Berezina^{1*}, D. J. Champion¹, P. C. C. Freire¹, T. M. Tauris^{1,2}, M. Kramer^{1,3},
A. G. Lyne³, B. W. Stappers³, L. Guillemot^{1,4,5}, I. Cognard^{4,5}, E. D. Barr¹,
R. P. Eatough¹, R. Karuppusamy¹, L. G. Spitler¹, G. Desvignes¹

¹Max-Planck-Institut für Radioastronomie, Auf dem Hügel 69, D-53121 Bonn, Germany

²Argelander-Institut für Astronomie, Universität Bonn, Auf dem Hügel 71, 53121 Bonn, Germany

³Jodrell Bank Centre for Astrophysics, School of Physics and Astronomy, The University of Manchester, Manchester M13 9PL, UK

⁴Laboratoire de Physique et Chimie de l'Environnement et de l'Espace, LPC2E, CNRS-Université d'Orléans, F-45071 Orléans, France

⁵Station de Radioastronomie de Nançay, Observatoire de Paris, CNRS/INSU, F-18330 Nançay, France

Accepted XXX. Received YYY; in original form ZZZ

ABSTRACT

We report the discovery and the results of follow-up timing observations of PSR J2045+3633 and PSR J2053+4650, two binary pulsars found in the Northern High Time Resolution Universe pulsar survey being carried out with the Effelsberg radio telescope. Having spin periods of 31.7 ms and 12.6 ms respectively, and both with massive white dwarf companions, $M_c > 0.8 M_\odot$, the pulsars can be classified as mildly recycled. PSR J2045+3633 is remarkable due to its orbital period (32.3 days) and eccentricity $e = 0.01721244(5)$ which is among the largest ever measured for this class. After almost two years of timing the large eccentricity has allowed the measurement of the rate of advance of periastron at the $5\text{-}\sigma$ level, $0.0010(2)^\circ \text{ yr}^{-1}$. Combining this with a detection of the orthometric amplitude of the Shapiro delay, we obtained the following constraints on the component masses (within general relativity): $M_p = 1.33^{+0.30}_{-0.28} M_\odot$, and $M_c = 0.94^{+0.14}_{-0.13} M_\odot$. PSR J2053+4650 has a 2.45-day circular orbit inclined to the plane of the sky at an angle $i = 85.0^{+0.8}_{-0.9}$ deg. In this nearly edge-on case the masses can be obtained from the Shapiro delay alone. Our timing observations resulted in a significant detection of this effect giving: $M_p = 1.40^{+0.21}_{-0.18} M_\odot$, and $M_c = 0.86^{+0.07}_{-0.06} M_\odot$.

Key words: pulsars: general – pulsars: binaries – pulsars: individual (PSR 2045+3633) – pulsars: individual (PSR 2053+4650)

1 INTRODUCTION

The discovery rate of binary pulsars has been rapidly increasing over the last decade and the population currently includes ~ 250 systems (Manchester et al. 2005). There is a large diversity among the nature of the companion stars and the characteristics of both the pulsars and their orbits (e.g. Tauris 2011). The companion stars detected so far are either non-degenerate main-sequence stars, semi-degenerate (and hydrogen rich) dwarfs, helium white dwarfs (He WDs), carbon-oxygen (CO) or oxygen-neon-magnesium (ONeMg) WDs, or neutron stars (NSs). Some pulsars are found with

planets (e.g. PSR B1257+12, Wolszczan & Frail 1992), and some are members of a triple system (e.g. PSR J0337+1715, Ransom et al. 2014).

The vast majority of the observed binary radio pulsars have been recycled via accretion of mass and angular momentum from a companion star (Bhattacharya & van den Heuvel 1991; Tauris & van den Heuvel 2006), often leading to formation of a millisecond pulsar (MSP). Accreting pulsars are observable in X-rays (Bildsten et al. 1997) as low- (LMXB), intermediate- (IMXB) or high-mass X-ray binaries (HMXB), depending on the mass of the donor star. The initial mass of the donor star has an impact on the duration and stability of the mass-transfer phase and, hence, the

* E-mail: mberezina@mpifr-bonn.mpg.de

efficiency of the recycling process. This, in turn, determines the main properties of the recycled pulsar, in particular its spin period and spin-down rate, as well as the final orbital configuration. This can clearly be seen when examining these properties as a function of the compact companion type in the known MSP population (Tauris et al. 2012). (In the following, we discard binary pulsars observed in dense environments like globular clusters since these binaries are possibly formed via exchange encounters (e.g. Verbunt & Freire 2014) and therefore have a different formation history compared to binary pulsars in the Galactic disk.) For example, MSPs with low-mass He WD companions are often fully recycled (with spin periods, $P < 10$ ms, and period derivatives, $\dot{P} \lesssim 10^{-20}$), whereas MSPs with massive CO/ONeMg WDs are often only mildly recycled with $10 < P < 100$ ms and $10^{-20} < \dot{P} < 10^{-18}$. The most massive donor stars are found in HMXBs. If such systems remain bound after the second supernova (SN) explosion, they produce double NS systems. In wide-orbit HMXBs, the effective mass-transfer phase is so short that the first born NS only becomes a marginally recycled pulsar (Tauris et al. 2015), in some cases with a spin period exceeding 100 ms. A prime example of such a system is the double NS system PSR J1930–1852 (Swiggum et al. 2015) which hosts a mildly recycled pulsar with $P = 185$ ms and has an orbital period of 45 days.

Pulsars with a compact star companion represent the end-point of binary stellar evolution. Thus, we can use the observed characteristics of these systems as fossil records to learn about stellar evolution and binary interactions in their progenitor systems (Lazarus et al. 2014). MSPs with He WD companions, and which have been recycled via stable Roche-lobe overflow (RLO) in LMXBs, possess a unique correlation between the mass of the WD and the orbital period (e.g. Tauris & Savonije 1999; Istrate et al. 2014). Furthermore, for these systems the orbital eccentricities are also correlated with the orbital period (Phinney 1992; Phinney & Kulkarni 1994), such that binaries with short orbital periods are more circular in general. For double NS systems, it is even possible to put constraints on the properties of the second SN explosion (Wex et al. 2000; Ferdman et al. 2013, 2014; Tauris et al. 2015).

Recycled pulsars with CO/ONeMg WD companions (also known as intermediate-mass binary pulsars, IMBPs) were first recognized as a separate class by Camilo (1996). Initially, it was thought that all such binaries form via common-envelope (CE) evolution. This idea was based on the formation scenario for PSR J2145–0750 (Bailes et al. 1994) which was put forward by van den Heuvel (1994). However, it was later demonstrated (Tauris et al. 2000) that such intermediate-mass binary pulsar systems can also be formed without the need for CE evolution, in cases when the observed orbital period is larger than 3 days. For these wider systems, the formation process was most likely dynamically stable RLO in an IMXB.

Although some consensus in our understanding of binary pulsars is emerging, it is important to keep finding new systems that will challenge current ideas and bring forward new lines of research. The discovery of PSR J1614–2230 (Demorest et al. 2010), which is the first example of a fully recycled MSP with a CO WD companion – and the first NS with a precisely measured mass close to $2.0 M_{\odot}$ – came

somewhat as a surprise. Subsequently, detailed modelling by Lin et al. (2011) and Tauris et al. (2011), suggested that this system is the first known example of an IMXB system which produced a radio pulsar evolving via Case A RLO (i.e. mass transfer initiated while the donor star is still burning hydrogen in its core). Hence, a third possibility for producing a recycled pulsar with a CO/ONeMg WD is now accepted.

The number of pulsar binaries with CO/ONeMg WDs now exceeds 30 systems. Their orbital eccentricities can vary from the order of 10^{-6} to 10^{-2} . This large spread in eccentricity suggests different formation paths. With only a small number of such systems known with precisely measured masses of the stellar components (apart from: PSR J1614–2230 (Ransom et al. 2014), PSR J1802–2124 (Ferdman et al. 2010) and PSR J0621+1002 (Splaver et al. 2002a)), it is difficult to speculate more precisely about their previous evolution. The discovery of new NSs with massive WD companions, which allow for mass determinations, would help shed new light on the formation process. Furthermore, precise knowledge of the present pulsar mass – in combination with other system parameters available from pulsar timing and theoretically computed binary models – will make it possible to estimate the amount of accreted material (and hence to infer the birth mass of the NS), determine which binary interactions were at work, and, consequently, try to deduce the formation history of the system as a whole. As an additional bonus, precise mass measurements can also serve for constraining the equation-of-state of cold dense matter within NSs (Özel & Freire 2016).

Here, we present the discovery and follow-up timing of two new mildly recycled MSPs which appear to be promising for the aforementioned purposes. They were discovered in June 2014 in the Northern High Time Resolution Universe survey (Barr et al. 2013). The structure of the paper is as follows: In Section 2, we introduce the survey and the discoveries; in Section 3, we describe our timing campaigns; in Section 4, we present the results of timing and polarisation analysis, discuss the details of the performed mass measurements and speculate about the eccentricity-binary period relation for IMBPs, and, finally, in Section 5, we summarize our work.

2 MSP DISCOVERIES IN THE HTRU-NORTH SURVEY

2.1 HTRU-North

The Northern High Time Resolution Universe survey for pulsars and fast transients is being conducted with the 100-m Effelsberg radio telescope in Germany. It makes use of the 21-cm seven-pixel multibeam receiver and the polyphase filterbank backend providing a time resolution of $54 \mu\text{s}$ and a 300-MHz passband centered around 1.36 GHz and split into 512 channels.

Being a counterpart of the Southern survey (HTRU-South; Keith et al. 2010), it follows the same observing convention with the sky split into three regions (the only difference is the integration time): low Galactic latitudes - $|b| < 3.5^{\circ}$ where each sky pointing is observed for 25 minutes, medium Galactic latitudes - $|b| < 15^{\circ}$ with the integration time of 3 minutes and high Galactic latitudes - $|b| > 15^{\circ}$

with 1.5 minute integrations. Pointings located in and near the Galactic plane are expected to harbour the highest yield of interesting PSR-WD or DNS systems (or even exotic systems with black hole companions; e.g. [Belczynski et al. 2002](#)) that can be used for such scientific purposes as studying stellar evolution, testing general relativity, constraining the equation-of-state of supra-nuclear matter (e.g. [Lorimer 2008](#)). For this reason, we are currently concentrating on the mid-latitude region with 3-minute integration times as a shallow survey of the plane can speed up the discovery and further studies of the brightest pulsars.

The northern part of the plane (as well as the whole northern sky) visible from Effelsberg has not yet been investigated in the L-Band, except for some regions of overlap with other 21-cm surveys like PALFA (e.g. [Cordes et al. 2006](#); [Lazarus 2013](#)), whose declination range is limited leaving large areas of the Galaxy uncovered, or with the southern surveys (HTRU-South, PMPS - see, for example, [Lorimer et al. 2006](#)). A high observing frequency reduces the impact of interstellar medium effects (such as dispersion and scattering) allowing the Galactic plane to be probed more deeply for distant objects. This depth of scanning distinguishes the HTRU-North from and, at the same time, makes it complementary to the low-frequency Northern-sky surveys such as the 350-MHz GBNC (Stovall et al. 2014), GBT drift-scan (Karako-Argaman et al. 2015) or the 140-MHz LOFAR pulsar surveys (Coenen et al. 2014) and the all-sky Arecibo 327 MHz drift survey (Deneva et al. 2013a) which use the steep spectral index observed in most pulsars to detect nearby weak sources. The full description of the survey and previous discoveries can be found in [Barr et al. \(2013, 2017\)](#).

2.2 Discoveries, initial timing and first scientific goals

Each of the two new bright binary MSPs, PSR J2045+3633 and PSR J2053+4650 (see Fig. 1a, 1b), with spin periods 31.68 ms and 12.58 ms, respectively, was found in 3-minute integration filterbank data down-sampled by factors of four in time and two in frequency, as is usual for survey processing with the quick-look pipeline. This pipeline (see [Barr et al. 2013](#)) is intended to discover the brightest sources as soon as possible, almost in real time. For this reason it operates on the low-resolution version of the data. This pipeline is based on the Fourier transform routines that are typical in pulsar searching. Before searching for periodic candidates, it performs dedispersion with 406 dispersion measure (DM) trials in the range of 0-2975 pc cm⁻³ in order to correct for *a priori* unknown dispersive smearing caused by the propagation of the possible pulsar signal through the ionized interstellar medium. This procedure is sufficient to find most solitary pulsars. In case of pulsars in binary systems whose signals can be modulated by orbital acceleration, to recover the original signal, an additional step of trying many possible acceleration values may be necessary. This is especially crucial for highly relativistic systems in short orbits. As this task is time-consuming and computationally intensive, the quick-look pipeline does not perform it, thus, limiting our detectability of highly accelerated systems but it still remains sensitive to non-relativistic pulsar binaries with relatively high DMs, like PSR J2045+3633 and PSR

J2053+4650 (129.5 pc cm⁻³ and 98.08 pc cm⁻³, respectively).

Confirmation observations for both pulsars were performed with the Effelsberg telescope soon after the discovery. Data taken in search and baseband modes for five minutes on several occasions within two weeks after the confirmation showed Doppler-shift variations of the spin period caused by the orbital motion. The `fitorbit`¹ program was used to produce robust initial parameter estimations prior to commencement of pulsar timing observations. Having the ephemeris allowed us to carry out observations in coherent-dedispersion real-time folding mode provided by the PSRIX ([Lazarus et al. 2016](#)) backend. From these data the times-of-arrivals (TOAs) were produced with `psrchive`² tools for pulsar analysis by doing standard procedures of cross-correlating the corresponding profile (obtained by fully integrating the archive file in time and frequency) with a template generated with `paas`. The initial timing model was fit to the data with `TEMPO`³ software resulting in a phase-coherent timing solution.

These first results showed that both pulsars are in binary orbits (with periods of 32.3 days for PSR J2045+3633 and 2.45 days for PSR J2053+4650) with massive companions. Moreover, both systems looked promising for precise measurements of the masses of the components through determination of post-Keplerian parameters ([Taylor & Weisberg 1982](#)). PSR J2045+3633 has revealed an eccentricity $e = 0.0172$, making possible a measurement of the rate of periastron advance. PSR J2053+4650 seemed to be in a circular, but highly-inclined orbit allowing the possible detection of the Shapiro delay ([Shapiro 1964](#)) caused by the propagation of the pulsar signal in the gravitational field of the companion (the effect is most noticeable when the orbit is close to being visible edge-on, i.e. the orbital inclination angle $i \approx 90^\circ$). The low root-mean-square (rms) of the first timing residuals (30 to 40 μ s for each pulsar) indicated that significant measurements of these parameters could be made on a short-term basis (within a few years).

3 HIGH PRECISION TIMING AND ANALYSIS

Regular timing was started in September 2014. The general timing strategy (i.e., excluding special campaigns - see 3.1 and 3.2) for both pulsars was similar: they were systematically followed up with the Lovell, Effelsberg and - (since March 2015) - Nançay radio telescopes, with an observation lasting, on average, 30-60 minutes. At Jodrell Bank, the pulsars were observed almost daily during the first three weeks and later - once in 10-20 days, at Effelsberg - almost monthly since December 2014 until November 2015, at Nançay the cadence varied from every day to once in a few months. Observational parameters and the details of the recording systems are presented in Table 1.

The overall preparation procedure was the same for the data from all the observatories: using `psrchive` tools, the data from each telescope were cleaned of RFI, fully integrated in time and integrated in frequency to keep a number

¹ <https://github.com/gdesvignes/fitorbit/>

² <http://psrchive.sourceforge.net/>

³ <http://sourceforge.net/>

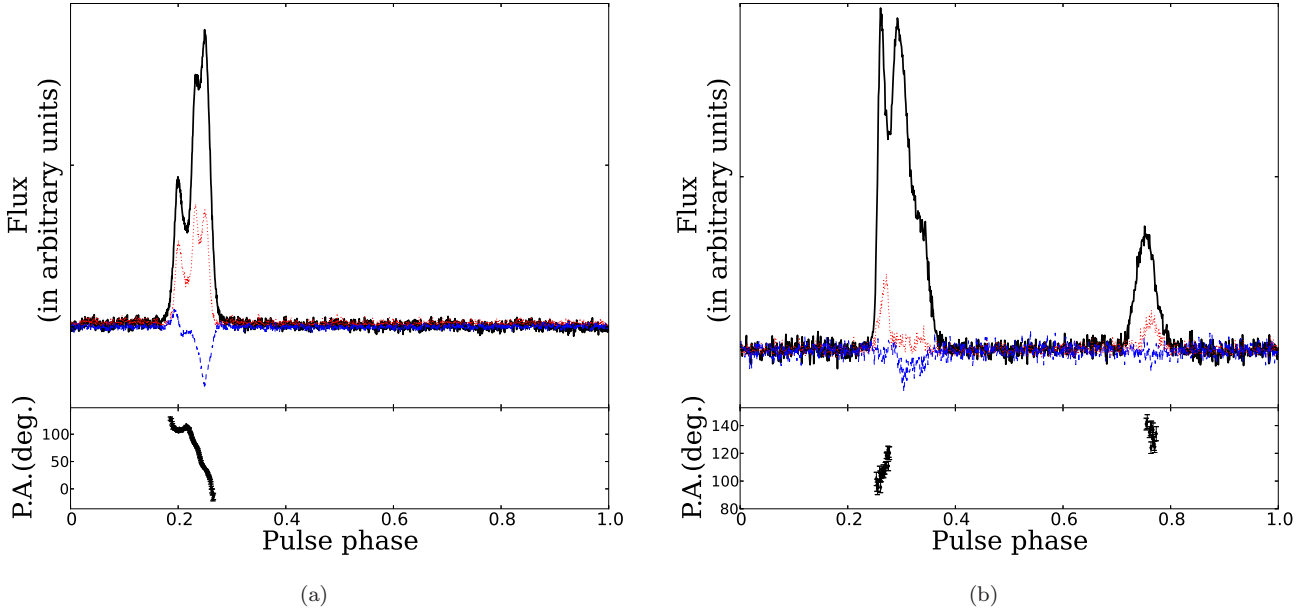


Figure 1. *Top* - Average pulse profiles with total intensity (black solid), linear (red dotted) and circular (blue dashed) polarisation vs. pulse phase for (a) PSR J2045+3633 obtained with the Arecibo telescope at 1430.8 MHz and (b) PSR J2053+4650 obtained with the Effelsberg telescope at 1347.5 MHz. *Bottom* - Position angle of linear polarisation vs. pulse phase.

Table 1. Timing observations of PSRs J2045+3633 and J2053+4650 with four telescopes

Telescope	Effelsberg	Jodrell Bank	Nançay	Arecibo
Backend	PSRIX	ROACH	NUPPI	PUPPI
Centre frequency (MHz)	1347	1520	1484	1430
Effective bandwidth (MHz)	240	384	512	600
Integration time (min)	30	30	10	11
Observation Parameters for PSR J2045+3633				
Number of TOAs	274	75	214	30
Number of frequency subbands (for producing TOAs)	4	1	4*	1
Weighted RMS of post-fit Timing Residuals (μ s)	5.388	4.356	7.541	1.110
EFAC	1.297	1.033	1.245	2.757
Date span (MJD)	56996-57284	56911-57538	57097-57506	57258-57294
Observation Parameters for PSR J2053+4650				
Number of TOAs	121	79	600	—
Number of frequency subbands (for producing TOAs)	2	1	4*	—
Weighted RMS of post-fit Timing Residuals (μ s)	3.078	3.128	5.189	—
EFAC	1.318	1.208	1.145	—
Date span (MJD)	56996-57145	56911-57538	57097-57490	—

* In most cases we kept four subbands but for some epochs the TOAs with uncertainties larger than 8μ s were excluded from the analysis resulting in two or three TOAs per epoch.

of subbands from one to four (depending on the observatory - see Table 1) and cross-correlated with a telescope-specific template to create TOAs. For the Lovell and Effelsberg observations we used an analytic template fit to the high signal-to-noise data created with the `paas` routine from `psrchive`. For Nançay the template was produced by adding 10 high signal-to-noise profiles for each pulsar, and the results from these additions were then smoothed. For the highest-quality Arecibo data the template was constructed from the average Arecibo pulse profiles over observed epochs. In our timing analysis we used `TEMP02` software package (Hobbs et al. 2006) refining the timing model by least-square fitting the parameters of the system. The TOAs from different observatories were converted to the Solar System barycentre using

the DE421 ephemeris. The details of fitting and models used are described in Section 4.3.

Given the eccentricity of PSR J2045+3633 and the fortuitous orbital inclination of PSR J2053+4650, we initiated special timing campaigns aiming to improve the measurement of the rate of advance of periastron and, possibly, the Shapiro delay for PSR J2045+3633, and the Shapiro delay for PSR J2053+4650, with a goal of constraining the masses of the pulsar and companion in both systems.

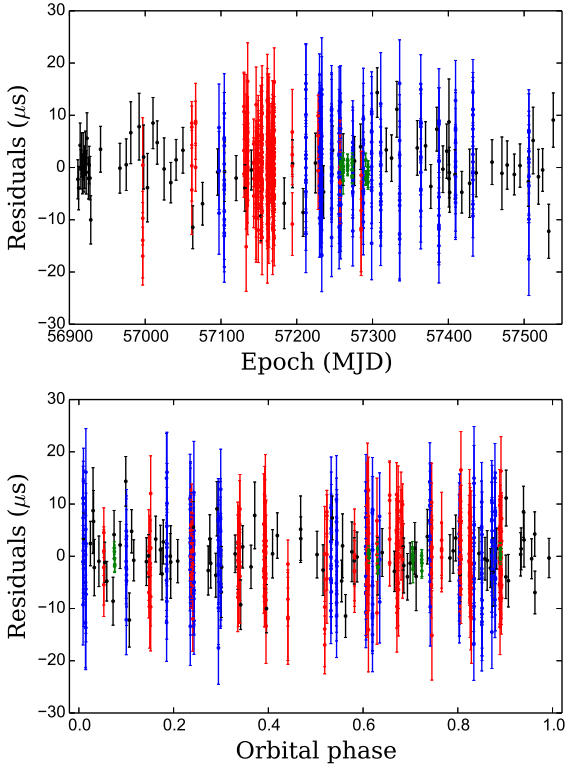


Figure 2. The top plot shows the post-fit timing residuals for PSR J2045+3633 as a function of MJD, the bottom plot - as a function of orbital phase. The residuals obtained from the data taken with different telescopes are marked with different colours: Jodrell Bank - black, Nançay - blue, Effelsberg - red, Arecibo - green. The error bars represent the $1\text{-}\sigma$ uncertainties of TOA measurements.

3.1 Special campaigns: PSR J2045+3633

For PSR J2045+3633 we conducted two full-orbit campaigns: one with the Effelsberg telescope and, in order to maximise our sensitivity, one with Arecibo.

The 32-day Effelsberg campaign took place in April-May 2015 and consisted of 10 four-hour observations at a central frequency of 1.4 GHz spread across the orbit. The data were recorded with the PSRIX (Lazarus et al. 2016) backend in its coherent-dedispersion real-time folding mode (the same system that is used for regular timing). The average TOA error was $3\ \mu\text{s}$.

The Arecibo campaign was held in August-September 2015 with the use of the L-band wide receiver. The data were coherently folded in real time with the PUPPI (Puerto Rico Ultimate Pulsar Processing Instrument) backend (Table 1). We performed 6 full-transit (55-minute) observations covering a part of the orbit. Due to some issues with the receiver, it was not possible to cover the whole orbit as planned but the data obtained (combined with all the other TOAs) still allowed us to measure the rate of advance of periastron ($\dot{\omega}$) at $5\text{-}\sigma$ level: $0.0010(2)^\circ\text{yr}^{-1}$ - and an indication of the Shapiro delay with 3- and $2\text{-}\sigma$ measurement of its orthometric amplitude and ratio: $h_3 = 1.0(3)\ \mu\text{s}$ and $\zeta = 0.6(3)$ respectively (see Section 4.3).

The average TOA error from this campaign was $0.29\ \mu\text{s}$

for the 11-minute observations fully scrunched in time and frequency. The higher precision of these TOAs compared to the ones from other telescopes made them overweighted in the overall timing analysis. For this reason, TOA uncertainties for a set of data from every observatory were multiplied by a factor (EFAC) between 1.033 and 2.757 (see Table 1) to achieve reduced $\chi^2 = 1$. EFACs of Jodrell Bank, Effelsberg and Nançay TOAs, slightly differing from unity, can be explained by the presence of RFI in the data whereas a much larger EFAC of much more precise Arecibo TOAs is probably an evidence of the intrinsic pulsar red noise. The overall timing residuals as a function of MJD and orbital phase are presented in Fig. 2.

3.2 Special campaign: PSR J2053+4650

For PSR J2053+4650 we performed two successive full-orbit campaigns with the Effelsberg telescope in the course of five days (April 29th-May 3rd 2015). On the first four days we observed it for four hours every day, and on the fifth day we took a twelve-hour session near the superior conjunction. This campaign helped to make a very significant Shapiro delay detection. Combined with the other TOAs (see Fig. 3), this resulted in the 22- and $66\text{-}\sigma$ measurement of the orthometric amplitude and orthometric ratio respectively: $h_3 = 3.23(15)\ \mu\text{s}$ and $\zeta = 0.918(14)$ (see Section 4.3).

4 RESULTS AND DISCUSSION

The resulting best-fit timing parameters for both pulsars are presented in Table 2. These include spin, astrometric and orbital parameters, as well as the derived masses of the systems.

4.1 Polarisation studies

At Effelsberg and Arecibo we performed a polarisation calibration observation with the noise diode prior to every pulsar observation. The diode signal was injected into the receiver feed horn at an angle of 45° to both polarisation probes when the telescope was 0.5° off source. These observations were used to calibrate the pulsar data with `pac` from `psrchive`. Several calibrated observations were then integrated to obtain a low-noise polarisation profile (Fig. 1a, 1b: for PSR J2045+3633 we present the Arecibo profile as it has much higher signal-to-noise ratio than the one from Effelsberg). The data for both pulsars were corrected for Faraday rotation with the values of rotation measure determined using `rmfit` from `psrchive` (see Table 2).

PSR J2045+3633 shows a significant degree of both linear and circular polarisation (Fig. 1a). Interpreted in the framework of polarisation features found in non-recycled pulsars (e.g. Lorimer & Kramer 2004), the change from a weak positive circular polarisation to significant negative polarisation suggests a central line of sight through the beam. This is consistent with the observed steep position angle (PA) swing. Despite the flat PA values in the leading part of the PA swing, it can be well described by a standard rotating vector model (RVM) fit, which in principle allows us to constrain the viewing geometry (e.g. Lorimer & Kramer 2004). The resulting χ^2 values from a least-squares fit of the

Table 2. Timing parameters for PSRs J2045+3633 and J2053+4650

Pulsar name	PSR J2045+3633	PSR J2053+4650	
Binary model	DDH	DDH	DD
Solar System ephemeris	DE421	DE421	DE421
Spin and astrometric parameters			
Right ascension, α (J2000)	20:45:01.50504(12)	20:53:52.62804(7)	
Declination, δ (J2000)	+36:33:01.4033(8)	+46:50:51.7181(4)	
Proper motion in RA, μ_α (mas yr ⁻¹)	-2.1(1.4)	-2.8(8)	
Proper motion in DEC, μ_δ (mas yr ⁻¹)	-2.3(8)	-5.4(5)	
Total proper motion, μ_{tot} (mas yr ⁻¹)	3.1(1.1)	6.1(5)	
Galactic longitude, l	77.83	86.86	
Galactic latitude, b	-3.93	1.30	
Pulse frequency, ν (s ⁻¹)	31.56382007686(1)	79.45162290069(1)	
First derivative of pulse frequency, $\dot{\nu}$ (s ⁻²)	-5.861(4) × 10 ⁻¹⁶	1.0875(6) × 10 ⁻¹⁵	
Spin period P (ms)	31.68184324854(1)	12.586275314350(2)	
Observed period derivative, \dot{P} (10 ⁻¹⁹ s s ⁻¹)	5.883(3)	1.7229(8)	
Dispersion measure, DM (pc cm ⁻³)	129.5477(17)	98.0828(6)	
Rotation measure, (rad m ⁻²)	-266(10)	-174(11)	
Binary Parameters			
Orbital period, P_b (days)	32.297845(1)	2.4524990114(2)	
Projected semi-major axis of the pulsar orbit, x (lt-s)	46.941885(11)	8.8042995(11)	8.8042996(11)
Epoch of periastron, T_0 (MJD)	57496.75108(3)	56911.113(3)	
Orbital eccentricity, e	0.01721244(5)	0.0000089(1)	
Longitude of periastron, ω (°)	320.7822(3)	266.7(4)	
Relativistic parameters and masses			
Rate of advance of periastron, $\dot{\omega}$ (° yr ⁻¹)	0.00105(14)	—	—
Orthometric amplitude, h_3 (μ s)	1.0(3)	3.23(15)	—
Orthometric ratio, ζ	0.6(3)	0.918(14)	—
Orbital inclination, i (°)	62 ⁺⁵ ₋₆	85.0 ^{+0.8} _{-0.9}	85.1 ^{+0.9} _{-0.7}
Mass function, f (M \odot)	0.1064621(2)	0.12182741(4)	
Total mass, M (M \odot)	2.28(45) (derived from $\dot{\omega}$)	—	2.23(24) ^a
Pulsar mass, m_p (M \odot)	1.33 ^{+0.30} _{-0.28} ^b	1.40 ^{+0.21} _{-0.18} ^b	1.38(18) ^a
Companion mass, m_c (M \odot)	0.94 ^{+0.14} _{-0.13} ^b	0.86 ^{+0.07} _{-0.06} ^b	0.85(6) ^a
Derived parameters			
DM-derived distance (NE2001) ^c , d (kpc)	5.51	4.12	
DM-derived distance (YMW16) ^d , d (kpc)	5.63	3.81	
Shklovskii's correction to period derivative, \dot{P} (10 ⁻²¹ s s ⁻¹)	4.2(3.1)	6.4(2.2)	
Shklovskii-corrected period derivative, \dot{P} (10 ⁻¹⁹ s s ⁻¹)	5.84(3)	1.66(2)	
Surface magnetic field strength, B_0 (10 ⁹ Gauss)	4.1	1.4	
Characteristic age, τ_c (Gyr)	0.85	1.15	

^a The pulsar and companion masses are calculated assuming GR from the range and shape of the Shapiro delay. The total mass is then calculated by summing these values.

^b The pulsar and companion masses derived from the Bayesian mapping (see sections about mass measurements).

^c We assume the uncertainty on the distance to be 25-30 %, what is commonly accepted when using the NE2001 model (Cordes & Lazio 2002), though these numbers represent a very average estimate and in general depend on the line of sight.

^d We assume the uncertainty on the distance to be 20-40 %, though it may be significantly underestimated (Yao et al. 2017).

Figures in parentheses are the nominal 1- σ TEMPO2 uncertainties in the least-significant digits quoted.

RVM to the PA swing produce the contours in the magnetic inclination angle (α) and viewing angle (i.e. angle between the spin axis and the observer's direction, ζ) plane shown in Fig. 4.

The correlation between α and ζ is not surprising and is well known; note that $\zeta = \alpha + \beta$, where β is the impact angle, i.e. the angle between magnetic axis and observer at the closest approach. In order to constrain the geometry further, we can utilize the constraints on the orbital inclination angle from pulsar timing, since for a pulsar beam of angular radius ρ to be visible to the observer, we find $|i - \zeta| \lesssim \rho$. The constraints on i and $180^\circ - i$ are correspondingly plotted in the upper panel of Fig. 4 as horizontal strips with a width identical to their uncertainties. For a pulsar with a filled emission beam, the observed pulse width

w is a function of α , ζ and ρ (e.g. Lorimer & Kramer 2004). For non-recycled pulsars, we find $\rho = k/\sqrt{P}$, where P is the pulse period and value of k depending weakly on frequency. The exact value differs between different authors, but for a width measured at a 10% intensity level k is typically about 6.3° (Kramer et al. 1994). Adopting this relationship and measuring a width of $w = 36^\circ$ we performed Monte Carlo simulations, where we drew ρ from a normal distribution centred on $k = 6.3^\circ$ with a width of 0.63° as a typical uncertainty reflecting both the uncertainty in k and the measured width. We also drew α from a flat distribution between 0 and 180°, while using another flat distribution for $\beta \leq \rho$ (i.e. the condition for the observer to register the beam). Testing 10 million combinations, we recorded those values of α where the observed width was consistent with

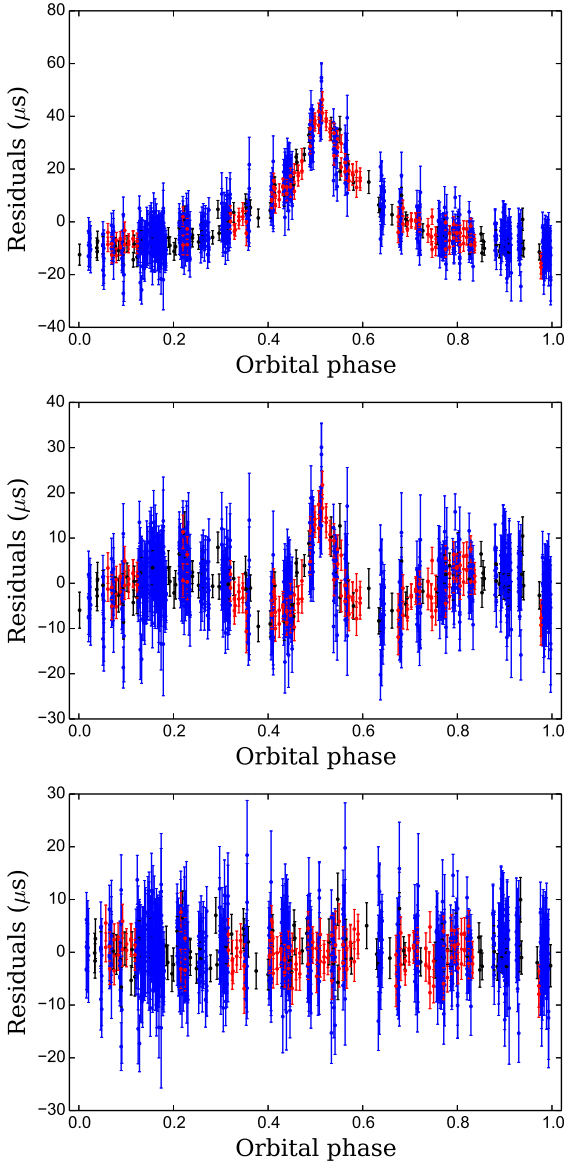


Figure 3. Timing residuals for PSR J2053+4650 as a function of orbital phase: the top plot shows residuals before fitting for Shapiro delay parameters, the bottom plot - after fitting. The middle plot shows timing residuals after fitting for Keplerian parameters: a part of the Shapiro delay is absorbed by this fit. The residuals obtained from the data taken with different telescopes are marked with different colours: Jodrell Bank - black, Nançay - blue, Effelsberg - red. The error bars represent the $1\text{-}\sigma$ uncertainties of TOA measurements.

the simulated values. This distribution of α is shown in the bottom panel of Fig. 4. Two preferred ranges of solutions near 50° and 130° are clearly visible. Dashed vertical lines indicate a $\pm 34\%$ range around the median value. Interestingly, the solutions for smaller α are more consistent with the joint constraints from the RVM fit and radio timing, indicating that the true underlying orbital inclination angle is $i \sim 60^\circ$ (rather than $180^\circ - 60^\circ = 120^\circ$). A corresponding RVM fit for $\alpha = 57^\circ$ and $\zeta = 60^\circ$ is shown in the small insert in the middle of the figure. In summary, radio timing, PA swing, and profile width data can all be explained in a self-

consistent geometric model, making assumptions that were derived from normal (non-recycled) pulsars.

We repeat the same procedure of fitting the RVM model for PSR J2053+4650. We can identify two main groups of significant PA values, clustering around longitudes of 100° and 280° , respectively (see insert in Fig. 5). We applied the same method as described above, but allow for the possibility that the two main clusters of PA values are separated by phase offsets of $\pm 90^\circ$ and $\pm 180^\circ$. This leads to various “islands” in the shown χ^2 plot. The indicated best fit solution that is consistent with a measurement of the orbital inclination angle (Table 2) is derived for zero offset between the two PA clusters. If we ignore the big “island” outside the alpha range, then the smaller inclination angle (87.5°) is slightly preferred but it is much less clear than in the case of PSR J2045+3633. What is clear from the given constraints is that the best solution is that of an orthogonal rotator, which is also consistent with the observation of an interpulse. Given this nearly orthogonal viewing geometry of the pulsar, it is to be expected that both solutions for the inclination should indeed have nearly equal probability.

4.2 Astrometric parameters

High-precision timing observations conducted for both binaries for almost 21 months gave us an opportunity to measure their proper motions. As can be seen from Table 2, for PSR J2045+3633 the proper motion is poorly constrained at $\mu_{\text{tot}} = 3.1 \pm 1.1 \text{ mas yr}^{-1}$. For PSR J2053+4650 the significance is higher at $\mu_{\text{tot}} = 6.1 \pm 0.5 \text{ mas yr}^{-1}$. Knowing the total proper motion, we can derive the transverse velocity from:

$$\frac{v_t}{\text{km s}^{-1}} = 4.74 \times \left(\frac{\mu_{\text{tot}}}{\text{mas yr}^{-1}} \right) \times \left(\frac{d}{\text{kpc}} \right), \quad (1)$$

where d is the distance to the pulsar. According to the NE2001 model described in Cordes & Lazio (2002), assuming the 25-30 % uncertainty on the DM-derived distance (although it should be noted that these uncertainties may be underestimated, see Deller et al. 2009), we obtain $v_t = 80 \pm 40 \text{ km s}^{-1}$ for PSR J2045+3633 and $v_t = 120 \pm 40 \text{ km s}^{-1}$ for PSR J2053+4650. Using the newer YMW20016 model (Yao et al. 2017) and assuming an average distance error of 40 % (though for individual sources it may be significantly larger), we get $v_t = 82 \pm 40 \text{ km s}^{-1}$ for PSR J2045+3633 and $v_t = 110 \pm 50 \text{ km s}^{-1}$ for PSR J2053+4650. The values obtained within the both models are consistent with each other and with the transverse velocities observed for the general population of binary MSPs (Hobbs et al. 2005; Gonzalez et al. 2011; Desvignes et al. 2016).

As demonstrated by Shklovskii (1970), the apparent period derivative of a pulsar is affected by its transverse motion as:

$$\frac{\dot{P}}{P} = \frac{1}{c} \times \frac{v_t^2}{d}, \quad (2)$$

where c is the speed of light. As can be seen from Table 2, currently the precision of the determined Shklovskii contribution is low for both MSPs: almost 1σ for PSR J2045+3633 and 3σ for PSR J2053+4650. However, they are two orders of magnitude below ($\sim 10^{-21} \text{ s}$) the observed \dot{P} values ($\sim 10^{-19} \text{ s}$), so they do not affect \dot{P} significantly. Nevertheless, we

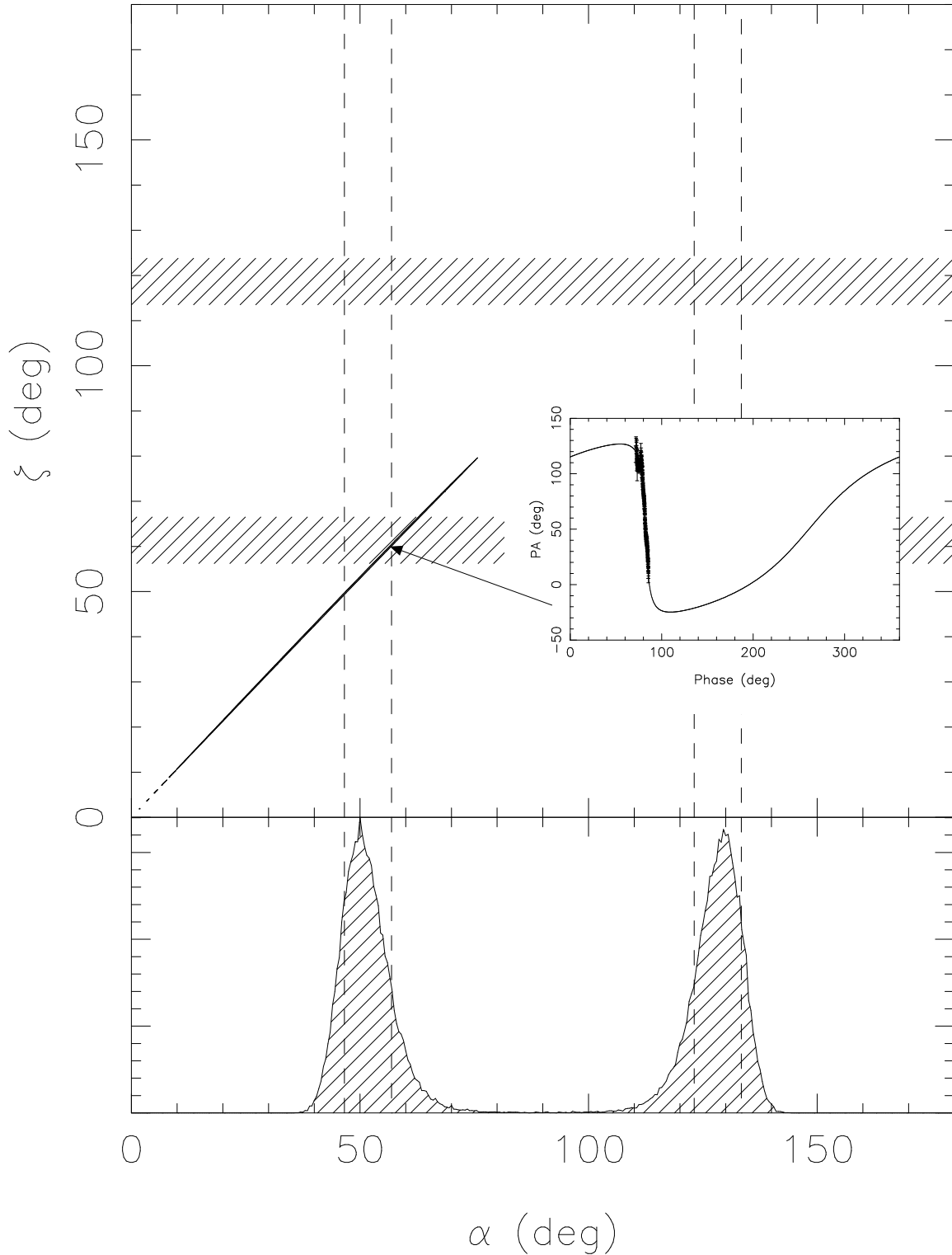


Figure 4. System geometry for PSR J2045+3633 as derived from a least-squares-fit of the Rotating Vector Model (RVM) to the position angle (PA) of the linearly polarized emission. The top panel shows the χ^2 contours from minimizing χ^2 by stepping through values of the magnetic inclination angle (α) and viewing angle ζ while simultaneously minimizing reference phase Φ_0 and reference position angle Ψ_0 of the RVM at each grid point. In order to constrain the geometry further in the presence of the correlation between α and ζ , we mark the constraints on the orbital inclination angle as horizontal strips (see text for details). Also, assuming a filled emission beam, we derive a distribution of magnetic inclination angles (lower panel) that is consistent with the observed pulse width (see text for details). The vertical dashed lines indicate a $\pm 34\%$ range around the median value of the two preferred solutions. The solutions for smaller α are more consistent with the joint constraints from the RVM fit and radio timing, indicating that the true underlying orbital inclination angle is $i \sim 60^\circ$ (rather than $180^\circ - 60^\circ = 120^\circ$). A corresponding RVM fit for $\alpha = 57^\circ$ and $\zeta = 60^\circ$ is shown in the small insert in the middle of the figure.

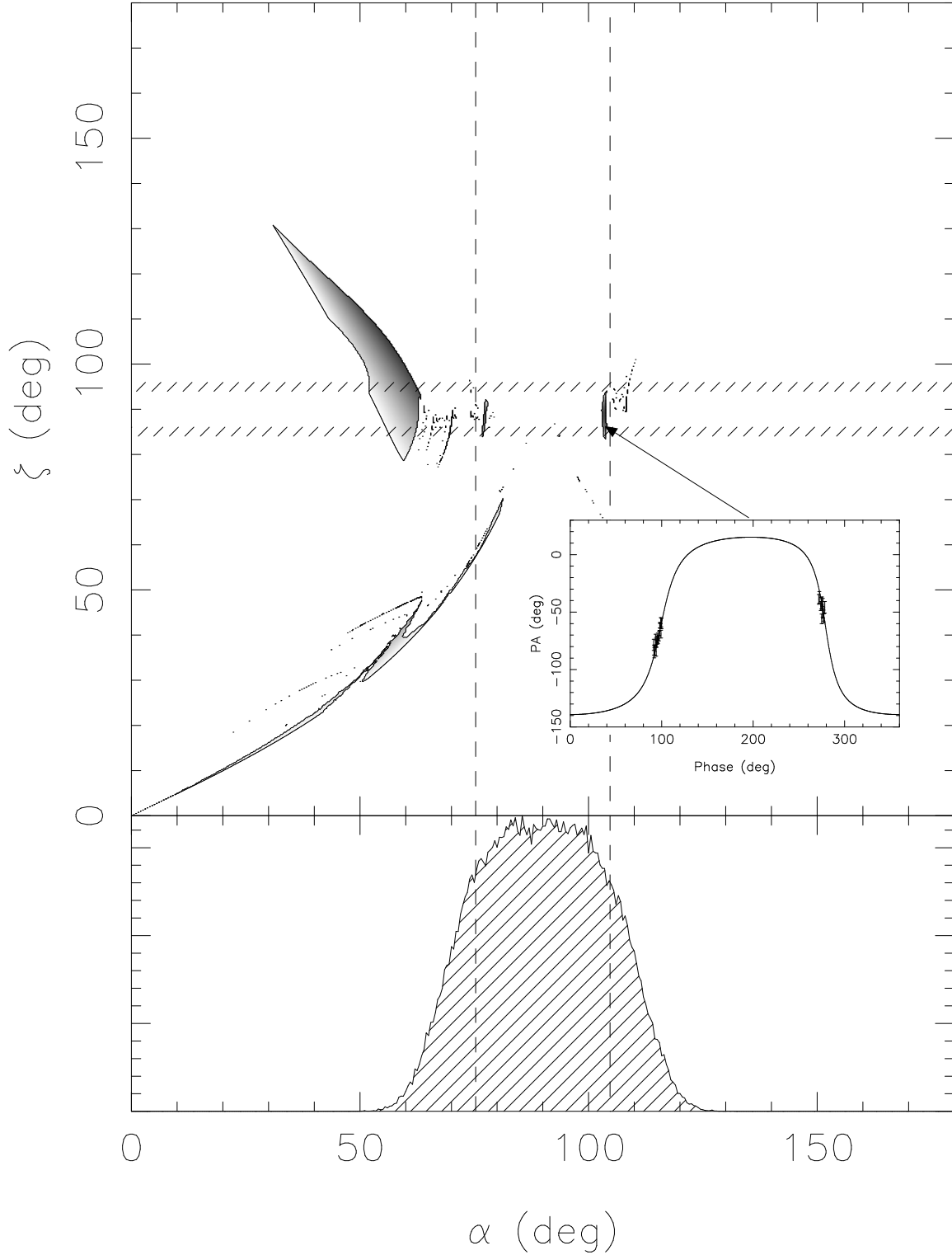


Figure 5. System geometry for PSR J2053+4650 as derived from least-squares-fit of the Rotating Vector Model to the position angle of the linearly polarized emission. See Figure 4 and text for details.

used the corrected values for estimating the magnetic field strengths and the characteristic ages.

4.3 Mass measurements and the nature of the companions

The masses of the components of the system are related to each other and to the Keplerian parameters of the orbit

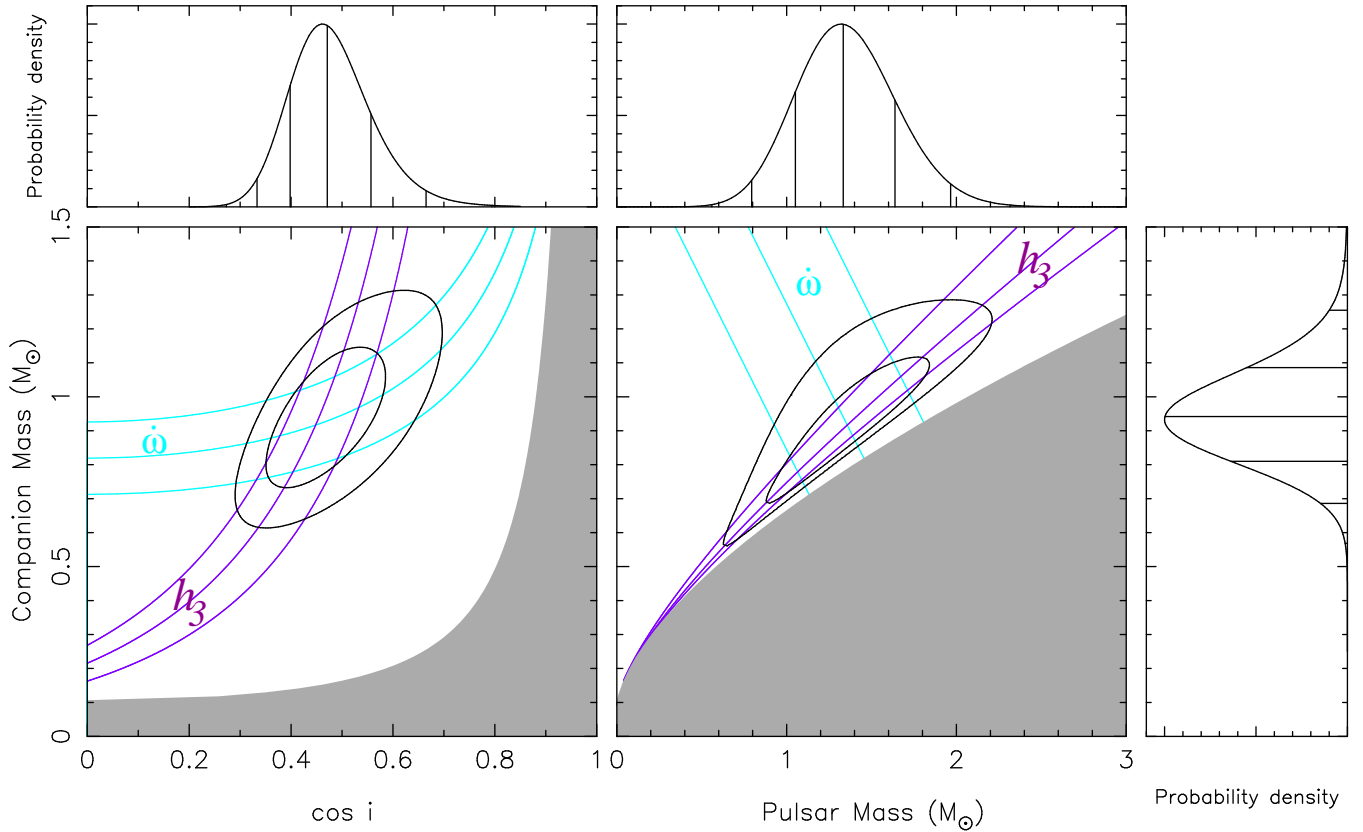


Figure 6. Constraints on the masses of the components and the orbital inclination angle for PSR J2045+3633. Each triplet of lines corresponds to the median values and $\pm 1\sigma$ uncertainties of the post-Keplerian parameters obtained within the DDH model: the rate of advance of periastron $\dot{\omega}$ (cyan) and the orthometric amplitude of the Shapiro delay, h_3 (purple) (the triplet for the orthometric ratio of the Shapiro delay ς is removed from the figure for better visual perception as it covers a wide region which includes both regions for $\dot{\omega}$ and h_3). The contour levels contain 68.27 and 95.45% of the 2-D probability density functions (pdfs) derived from the quality of the timing solution at each point on the $M_c - \cos i$ plane using the Shapiro delay together with an assumption that $\dot{\omega}$ can be fully described by general relativity to constrain the masses. The left plot shows the $M_c - \cos i$ plane with the gray region excluded by the physical constraint $M_p > 0$. The right plot shows $M_c - M_p$ plane with the gray region excluded by the mathematical constraint $\sin i \leq 1$. The top plots depict probability density functions for $\cos i$, M_p and the right marginal plot - for M_c , derived from marginalizing the 2-D pdf in the main panel for these quantities.

through the mass function (e.g. Lorimer & Kramer 2004):

$$f(M_p, M_c) = \frac{(M_c \sin i)^3}{(M_p + M_c)^2} = \frac{4\pi^2 x^3}{T_\odot P_b^2}, \quad (3)$$

where M_p and M_c are the pulsar and companion masses in units of a solar mass, i is the orbital inclination, x is the projected semi-major axis of the orbit in light seconds and $T_\odot \equiv GM_\odot c^{-3} = 4.9254909476412675 \mu\text{s}$ is a solar mass in time units (in the latter expression c is the speed of light and G is Newton’s gravitational constant). If two more equations with the same three unknown variables, M_p , M_c and $\sin i$, become available, it is possible to determine the masses of the pulsar and its companion. These equations can be found within the so-called Post-Keplerian (PK) formalism where a set of relativistic additions to the classical Keplerian parameters can be parameterized in a theory-independent way in various timing models.

If we assume GR to be the correct theory of gravity, then these Post-Keplerian (PK) parameters (such as the orbital period derivative \dot{P}_b , the advance of periastron $\dot{\omega}$, the gravitational redshift γ and the range r and shape s of the Shapiro delay) relate the component masses and the

Keplerian parameters (see Taylor & Weisberg 1982), thus, providing extra equations complementing Eq. 3. If two PK parameters are available, we can determine the component masses, if more PK parameters are available we can test the self-consistency of GR and other theories of gravity.

The total mass of the system can be obtained from the measurement of the periastron advance, $\dot{\omega}$, according to:

$$M_{\text{tot}} = \frac{1}{T_\odot} \left[\frac{\dot{\omega}}{3} (1 - e^2) \right]^{\frac{3}{2}} \left(\frac{P_b}{2\pi} \right)^{\frac{5}{2}}. \quad (4)$$

The component masses come from the measurement of the Shapiro delay. In the DD parameterization (Damour & Deruelle 1985, 1986), this is described by the “Range” $r = T_\odot M_c$ and “Shape” $s = \sin i$ parameters. In DDH parameterization (Freire & Wex 2010), we have the orthometric ratio and amplitude, respectively:

$$\varsigma = \frac{\sin i}{1 + \cos i}, \quad h_3 = r \varsigma^3. \quad (5)$$

The latter parameterization has the advantage of a smaller correlation between the parameters and also better describes the regions of the $M_c - \sin i$ plane where the parameters of

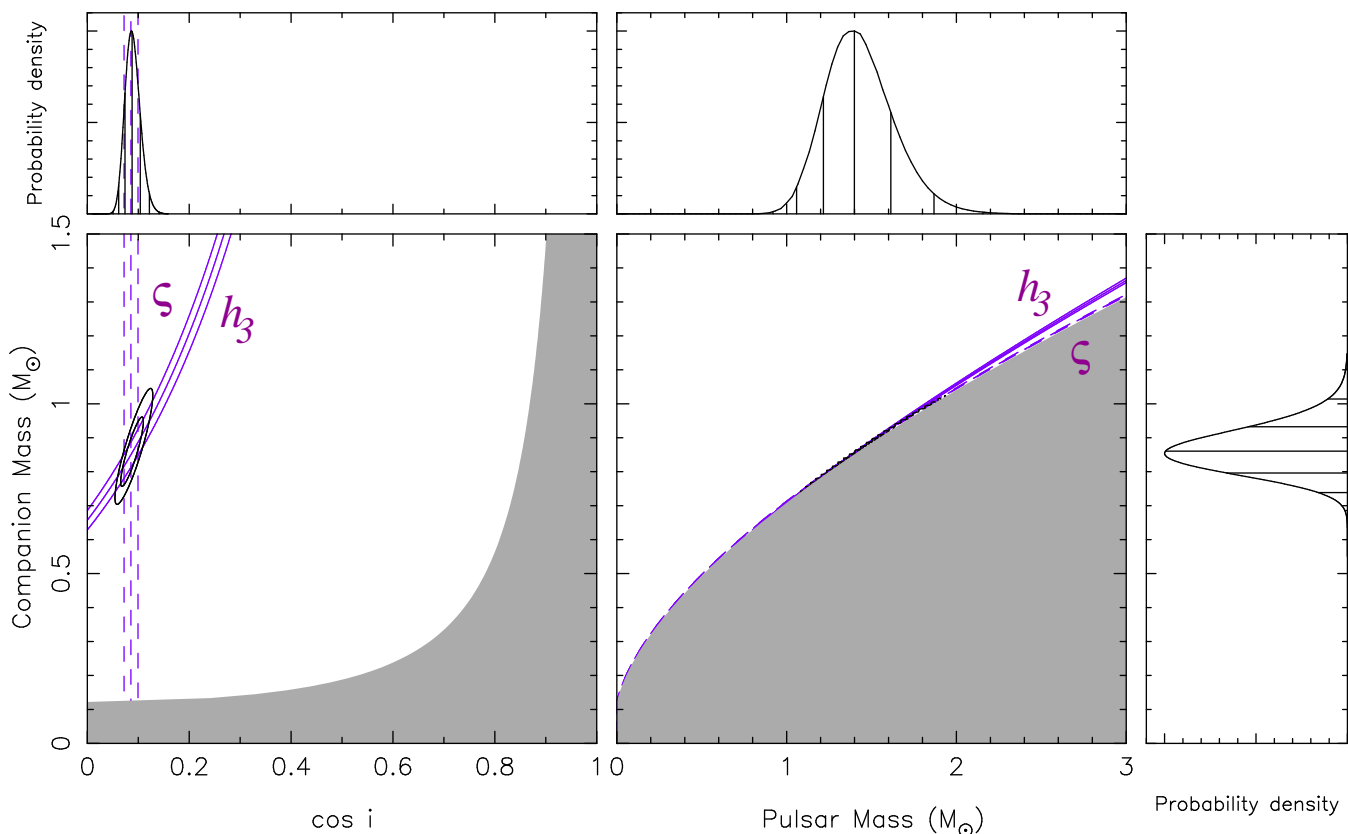


Figure 7. Constraints on the masses of the components and the orbital inclination angle for PSR J2053+4650 in the same manner as in Fig. 6. The only difference is in the PK parameters used to constrain the masses: in this case the orthometric amplitude h_3 (solid purple) and the orthometric ratio of the Shapiro delay ζ (dashed purple).

the system are. For this reason, when other PK effects are also known, then this parameterization provides a better test of GR.

4.3.1 PSR J2045+3633

For PSR J2045+3633 we have used the DDH model to measure the PK parameters $\dot{\omega}$, h_3 and ζ . From the measurement of $\dot{\omega}$ we derived the total mass $M_{\text{tot}} = 2.28(45) M_{\odot}$ using Eq. 4.

We can estimate approximately the masses of the individual components from the intersection of the h_3 and $\dot{\omega}$ curves⁴ in Fig. 6. To do this robustly, we performed a Bayesian χ^2 analysis in the $M_c - \cos i$ plane in the fashion described in Splaver et al. (2002b). For each point in this plane, we calculated the Shapiro delay parameters and the rate of advance of periastron using the specifications of general relativity. Keeping these fixed, we fitted for the spin, astrometric and Keplerian parameters tracking the post-fit χ^2 (see Fig. 6). From this χ^2 map we derived a 2-D probability distribution function (pdf) that was then translated into a 2-D pdf in the $M_c - M_p$ plane using Eq. 3. We then marginalize the 2-D pdfs to derive 1-D pdfs for M_c , $\cos i$ and M_p .

As can be seen from Table 2 and Fig. 6, the current

precision of the Shapiro delay measurement, even combined with $\dot{\omega}$, does not allow us to constrain the masses precisely. This is a consequence of the orbit not being highly inclined, with $i = 62_{-6}^{+5}^{\circ}$. The best-fit mass values within 1σ -band are: $M_p = 1.33_{-0.28}^{+0.30} M_{\odot}$, $M_c = 0.94_{-0.13}^{+0.14} M_{\odot}$. The mass of the pulsar is not yet precise enough for any conclusions, however, it is clear that the companion is either a heavy CO or ONeMg WD, as implied by the large mass function of the system.

Continued timing with a special focus on observations near the superior conjunction will greatly improve the precision of the Shapiro delay detection, but even greater improvements will arise from the fast-improving measurement of $\dot{\omega}$, for which the uncertainty is proportional to $T^{-3/2}$ (where T is the temporal span of the timing data).

Given the large orbital period of PSR J2045+3633 ($P_b = 32.3$ days), this system probably did not evolve via CE (if so, the envelope of the WD progenitor star must have been very weakly bound at the onset of the CE because of the small degree of orbital in-spiral). This system might instead have formed by stable Case B RLO in an IMXB system (Tauris et al. 2000). It is worth noting that the orbital configuration is also compatible with theoretical modelling of IMXBs producing pulsars with massive WDs. However,

constraints from the measurement of $\sin i$ and M_c are too wide to give any useful mass constraints.

⁴ Note that this is not possible in the r - s parameterization, where

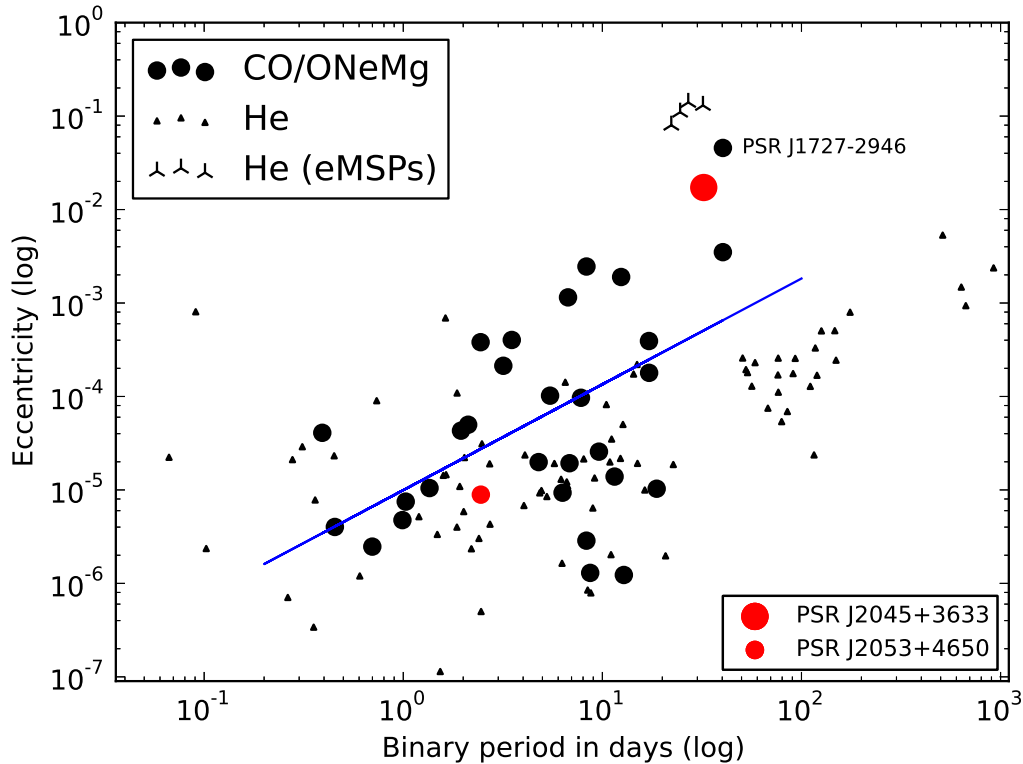


Figure 8. Location of the two new MSPs on the $P_b - ecc$ diagram for the population of binary pulsars with WD companions and spin periods < 100 ms. The blue line is a linear regression fit for IMBPs (CO/ONeMg WD companions).

the large orbital period could possibly be accounted for by changing the assumptions of the specific orbital angular momentum carried away by the material lost from the system during RLO.

4.3.2 PSR J2053+4650

For this system, the high orbital inclination and large companion mass yield a strong signature of the Shapiro delay (Fig. 3) allowing mass measurements from this effect alone. We fitted the timing data with both DD and DDH models. The masses derived from the range and shape parameters measured within the DD model are consistent with the values obtained from a Bayesian analysis (Fig. 7) similar to that described in Section 4.3.1 performed within the DDH model: $M_p = 1.40^{+0.21}_{-0.18} M_\odot$, $M_c = 0.86^{+0.07}_{-0.06} M_\odot$. The companion is most likely a heavy CO WD, or possibly an ONeMg WD. For this system, although we will not be able to measure any other PK parameters in the near future (a couple of years); it is possible that $\dot{\omega}$ might be measurable in the distant future (tens of years).

The combination of a short orbital period ($P_b = 2.45$ days) and a massive WD companion suggests that this system formed via CE evolution from an IMXB with a donor star on the asymptotic giant branch, e.g. following the scenario suggested by van den Heuvel (1994).

4.4 Eccentricity of PSR J2045+3633

For the majority of known IMBPs observed, eccentricities range from 10^{-6} to 10^{-3} (see Fig. 8). This is certainly the case for one of our new binary systems, PSR J2053+4650. However, some systems have larger eccentricities, one of them being PSR J0621+1002 (Splaver et al. 2002b) which has $e = 0.00245744(5)$. In 2015, a presumed IMBP, PSR J1727-2946, was discovered with an orbital period of 40 days and an eccentricity of $e = 0.04562943(16)$ (see Lorimer et al. 2015), even larger than that of PSR J2045+3633 ($e = 0.01721244(5)$).

Looking at Fig. 8, based on the data from the ATNF catalogue⁵, we could in principle say that the relatively high orbital eccentricities of PSR J2045+3633 and PSR J1727-2946 are the result of a smooth trend of increasing orbital eccentricity with orbital period among the systems with massive WD companions. Indeed, the correlation shown as a blue line in Fig. 8 was obtained as a result of a linear regression fit to the observed data (in logarithmic scale) with $R^2 = 0.515$, $p = 0.003$ and $stderr = 0.35$. This low significance for the regression is not surprising if we take into account the large spread in eccentricities for a given orbital period.

Given the three different formation channels proposed

⁵ <http://www.atnf.csiro.au/people/pulsar/psrcat/>; Manchester et al. (2005)

for IMBPs (see Section 1), the scatter in Fig. 8 could simply reflect different origins of these systems.

It is interesting to note that the orbital periods of PSR J2045+3633 and PSR J1727–2946 are close to those of the anomalously eccentric MSP–He WD systems (eMSPs): PSR J1946+3417 (Barr et al. 2013, 2017), PSR J2234+0611 (Deneva et al. 2013b; Antoniadis et al. 2016), PSR J1950+2414 (Knispel et al. 2015) and PSR J0955–6150 (Camilo et al. 2015). Very few (if any) circular systems are observed in this orbital period range (sometimes dubbed the “Camilo gap” first noticed in Camilo 1996). Although we cannot see any common physical mechanism, it is possible that for IMBPs there might also be an eccentricity anomaly at these orbital periods. This would be very surprising: all of the scenarios put forward to explain the eccentric MSP–He WD systems with orbital periods between 22 and 32 days (Freire & Tauris 2014; Antoniadis 2014; Jiang et al. 2015) make those predictions for low-mass He WD companions only.

Further discoveries of IMBPs with these orbital periods and larger will be necessary for determining whether IMBPs follow a smooth trend in the $P_b - ecc$ diagram, or whether there possibly is a universal eccentricity anomaly for all binary pulsars with orbital periods between 20 and 40 days.

5 SUMMARY AND CONCLUSIONS

We have presented two binary MSPs discovered in the Northern High Time Resolution Universe pulsar survey. As shown by the timing solutions, we have added two new members to the population of intermediate-mass binary pulsars. While PSR J2053+4650 is a standard representative of this population, PSR J2045+3633, with its relatively large eccentricity $e = 0.0172$, appears to be atypical (there are only a few other systems with eccentricities of the same order) and especially interesting for studying stellar evolution.

Both systems are promising for precise mass measurements of their components. Current constraints on the pulsar masses are $1.33^{+0.30}_{-0.28} M_\odot$ for PSR J2045+3633 and $1.40^{+0.21}_{-0.18} M_\odot$ for PSR J2053+4650 where the median values are in agreement with the assumption that the masses of mildly recycled pulsars should be close to their birth values $\sim 1.35 M_\odot$ since they accreted little matter from their massive companions. The precision of measurements will be improved with further timing. Moreover, in the case of PSR J2045+3633, three post-Keplerian parameters (the periastron advance and two Shapiro delay parameters) can be measured with high precision in the near future providing additional constraints. The low rms of timing residuals and sharp profiles of both pulsars suggest that they may be useful for pulsar timing arrays.

ACKNOWLEDGEMENTS

The Arecibo Observatory is operated by SRI International under a cooperative agreement with the National Science Foundation (AST-1100968), and in alliance with Ana G. Méndez-Universidad Metropolitana, and the Universities Space Research Association. The part of this work is based on observations with the 100-m telescope of the MPIfR

(Max-Planck-Institut für Radioastronomie) at Effelsberg. The observations using the Lovell Telescope at Jodrell Bank are supported by a consolidated grant from the STFC in the UK. The Nançay radio observatory is operated by the Paris Observatory, associated with the French Centre National de la Recherche Scientifique (CNRS). We also acknowledge financial support from the ‘Gravitation, Références, Astronomie, Métrologie’ (GRAM) national programme of CNRS/INSU, France.

REFERENCES

- Antoniadis J., 2014, *ApJ*, **797**, L24
- Antoniadis J., Kaplan D., Stovall K., Freire P. C., Deneva J. S., Koester D., Jenet F., Martinez J., 2016, preprint, ([arXiv:1601.08184](https://arxiv.org/abs/1601.08184))
- Bailes M., et al., 1994, *ApJ*, **425**, L41
- Barr E. D., et al., 2013, *MNRAS*, **435**, 2234
- Barr E. D., Freire P. C. C., Kramer M., Champion D. J., Berezhina M., Bassa C. G., Lyne A. G., Stappers B. W., 2017, *MNRAS*, **465**, 1711
- Belczynski K., Kalogera V., Bulik T., 2002, *ApJ*, **572**, 407
- Bhattacharya D., van den Heuvel E. P. J., 1991, *Physics Reports*, **203**, 1
- Bildsten L., et al., 1997, *ApJS*, **113**, 367
- Camilo F., 1996, in S. Johnston, M. A. Walker, & M. Bailes ed., *Astronomical Society of the Pacific Conference Series Vol. 105*, IAU Colloq. 160: Pulsars: Problems and Progress. pp 539–+
- Camilo F., et al., 2015, *ApJ*, **810**, 85
- Coenen T., et al., 2014, *A&A*, **570**, A60
- Cordes J. M., Lazio T. J. W., 2002, *ArXiv Astrophysics e-prints*,
- Cordes J. M., et al., 2006, *ApJ*, **637**, 446
- Damour T., Deruelle N., 1985, *Ann. Inst. Henri Poincaré Phys. Théor.*, Vol. 43, No. 1, p. 107 - 132, **43**, 107
- Damour T., Deruelle N., 1986, *Ann. Inst. Henri Poincaré Phys. Théor.*, Vol. 44, No. 3, p. 263 - 292, **44**, 263
- Deller A. T., Tingay S. J., Bailes M., Reynolds J. E., 2009, *ApJ*, **701**, 1243
- Demorest P. B., Pennucci T., Ransom S. M., Roberts M. S. E., Hessels J. W. T., 2010, *Nature*, **467**, 1081
- Deneva J. S., Stovall K., McLaughlin M. A., Bates S. D., Freire P. C. C., Martinez J. G., Jenet F., Bagchi M., 2013a, *ApJ*, **775**, 51
- Deneva J. S., Stovall K., McLaughlin M. A., Bates S. D., Freire P. C. C., Martinez J. G., Jenet F., Bagchi M., 2013b, *ApJ*, **775**, 51
- Desvignes G., et al., 2016, *MNRAS*, **458**, 3341
- Ferdman R. D., et al., 2010, *ApJ*, **711**, 764
- Ferdman R. D., et al., 2013, *ApJ*, **767**, 85
- Ferdman R. D., et al., 2014, *MNRAS*, **443**, 2183
- Freire P. C. C., Tauris T. M., 2014, *MNRAS*, **438**, L86
- Freire P. C. C., Wex N., 2010, *MNRAS*, **409**, 199
- Gonzalez M. E., et al., 2011, *ApJ*, **743**, 102
- Hobbs G., Lorimer D. R., Lyne A. G., Kramer M., 2005, *MNRAS*, **360**, 974
- Hobbs G. B., Edwards R. T., Manchester R. N., 2006, *MNRAS*, **369**, 655
- Istrate A. G., Tauris T. M., Langer N., Antoniadis J., 2014, *A&A*, **571**, L3
- Jiang L., Li X.-D., Dey J., Dey M., 2015, *ApJ*, **807**, 41
- Karako-Argaman C., et al., 2015, *ApJ*, **809**, 67
- Keith M. J., et al., 2010, *MNRAS*, **409**, 619
- Knispel B., et al., 2015, *ApJ*, **806**, 140
- Kramer M., Wielebinski R., Jessner A., Gil J. A., Seiradakis J. H., 1994, *A&AS*, **107**
- Lazarus P., 2013, in *IAU Symposium*. pp 35–40

- Lazarus P., et al., 2014, *MNRAS*, **437**, 1485
- Lazarus P., Karuppusamy R., Graikou E., Caballero R. N., Champion D. J., Lee K. J., Verbiest J. P. W., Kramer M., 2016, *MNRAS*, **458**, 868
- Lin J., Rappaport S., Podsiadlowski P., Nelson L., Paxton B., Todorov P., 2011, *ApJ*, **732**, 70
- Lorimer D. R., 2008, *Living Reviews in Relativity*, 11
- Lorimer D. R., Kramer M., 2004, *Handbook of Pulsar Astronomy*
- Lorimer D. R., et al., 2006, *MNRAS*, **372**, 777
- Lorimer D. R., et al., 2015, *MNRAS*, **450**, 2185
- Manchester R. N., Hobbs G. B., Teoh A., Hobbs M., 2005, *AJ*, **129**, 1993
- Özel F., Freire P., 2016, *ARA&A*, **54**, 401
- Phinney E. S., 1992, *Royal Society of London Philosophical Transactions Series A*, **341**, 39
- Phinney E. S., Kulkarni S. R., 1994, *ARA&A*, **32**, 591
- Ransom S. M., et al., 2014, *Nature*, **505**, 520
- Shapiro I. I., 1964, *Physical Review Letters*, **13**, 789
- Shklovskii I. S., 1970, *Soviet Ast.*, **13**, 562
- Splaver E. M., Nice D. J., Arzoumanian Z., Camilo F., Lyne A. G., Stairs I. H., 2002a, *ApJ*, **581**, 509
- Splaver E. M., Nice D. J., Arzoumanian Z., Camilo F., Lyne A. G., Stairs I. H., 2002b, *ApJ*, **581**, 509
- Stovall K., et al., 2014, *ApJ*, **791**, 67
- Swiggum J. K., et al., 2015, *ApJ*, **805**, 156
- Tauris T. M., 2011, in Schmidtobreick L., Schreiber M. R., Tappert C., eds, *Astronomical Society of the Pacific Conference Series Vol. 447, Evolution of Compact Binaries*. p. 285 ([arXiv:1106.0897](https://arxiv.org/abs/1106.0897))
- Tauris T. M., Savonije G. J., 1999, *A&A*, **350**, 928
- Tauris T. M., van den Heuvel E. P. J., 2006, *Formation and evolution of compact stellar X-ray sources*. Cambridge University Press, pp 623–665
- Tauris T. M., van den Heuvel E. P. J., Savonije G. J., 2000, *ApJ*, **530**, L93
- Tauris T. M., Langer N., Kramer M., 2011, *MNRAS*, **416**, 2130
- Tauris T. M., Langer N., Kramer M., 2012, *MNRAS*, **425**, 1601
- Tauris T. M., Langer N., Podsiadlowski P., 2015, *MNRAS*, **451**, 2123
- Taylor J. H., Weisberg J. M., 1982, *ApJ*, **253**, 908
- Verbunt F., Freire P. C. C., 2014, *A&A*, **561**, A11
- Wex N., Kalogera V., Kramer M., 2000, *ApJ*, **528**, 401
- Wolszczan A., Frail D. A., 1992, *Nature*, **355**, 145
- Yao J. M., Manchester R. N., Wang N., 2017, *ApJ*, **835**, 29
- van den Heuvel E. P. J., 1994, *A&A*, **291**, L39

This paper has been typeset from a $\text{\TeX}/\text{\LaTeX}$ file prepared by the author.